MODELLING LOCALISED FAILURE OF REINFORCED CONCRETE SLABS IN FIRE

Xinmeng Yu[1,*], Zhaohui Huang[1], Ian Burgess[1], and Roger Plank[2]

[1] Department of Civil & Structural Engineering, University of Sheffield, Sheffield S1 3JD, UK
[2] School of Architectural Studies, University of Sheffield, Sheffield S10 2TN, UK

Keywords: Reinforced concrete; slabs; Localised failure; Embedded FEM; Weak discontinuity; Numerical modelling; Fire condition; Layered slab FE model.

ABSTRACT

It has been observed from a series of tests on simply supported reinforced concrete slabs that the main failure mode of the slabs at large deflections is due to the formation of large discrete tension cracks. This localised failure was also previously observed in the Cardington full-scale fire tests. Smeared cracking models can be used successfully to predict the global behaviour of concrete slabs subject to large deflections, but they are not ideal for predicting the formation of localised cracks. Discrete cracking models usually assume that cracks form only along element edges, so that continuous re-meshing is required during the analysis. Consequently, the results are mesh-dependent and the computing cost is high. In recent years, meshless finite element procedures, such as embedded (EFEM) and extended (XFEM) approaches, have been widely used for modelling crack initiation and growth in structural members. Most of the available meshless models developed are either based on in-plane loading conditions or are confined to thin shells with assumed full-depth cracks. However, for a reinforced slab, transverse loading causes coupled stretching and bending of the slab; cracks are usually initiated at discrete positions and then propagated, until at last some localised full-depth cracks have been formed.

In this research, a layered procedure with embedded weak discontinuity is developed to model localised failure in reinforced concrete slabs subjected to extreme loading conditions. It can be seen that the numerical predictions of this model, in terms of both deflection and cracking pattern, agree well with test results at both ambient and elevated temperatures. The model developed is not sensitive to the mesh size or to the aspect ratio of the slab.

1. INTRODUCTION

A series of small-scale thin reinforced concrete slabs have recently been tested at both ambient and elevated temperatures at the University of Manchester [1] and the University of Sheffield [2]. The slabs were uniformly loaded, with all four edges simply supported. It was observed that the slabs could undergo large deformations at elevated temperatures, far beyond the design loads given by yield line theory. This is due to the development of secondary load-carrying mechanisms, such as tensile membrane action, after conventional small-deflection strength limits have been reached. The main failure mode of the slabs at large deflections is the

* Corresponding author - Departament of Civil and Structural Engineering. University of Sheffield. UK. Tel.: +44 114 222 5362 Fax: +44 114 222 5700. e-mail: x.m.yu@sheffield.ac.uk

formation of large discrete cracks [1], which means that their integrity condition of fire resistance as separating elements is violated. This localised failure of slabs subject to large deflections had previously been observed in the Cardington full-scale fire tests.

In the past decade, several numerical models have been developed to study the structural behaviour of reinforced concrete slabs in fire conditions [3-5]. All of these models use the smeared cracking assumption to model the failure of concrete. These simulate well the global behaviour of slabs subject to large deflections, but this damage model cannot predict localisation of the failure. It is clear that, when a large crack is formed, the criterion of structural integrity is violated, although global stability of the structure may still be maintained. It is therefore important to develop a numerical procedure in which both structural stability and integrity can be assessed, so that a meaningful structural failure point can be identified by numerical analysis.

Early models used for nonlinear finite element analysis of concrete structures attempted to model discrete cracking using linear elastic fracture mechanics (LEFM). In these models discrete cracking was introduced explicitly as an opening in the finite element mesh, usually located along the element edges. Consequently, continuous re-meshing was required during analysis, and inevitably the results were mesh-dependent. In recent years, there has been a great interest in developing mesh-independent, or meshless, finite element procedures for modelling of crack initiation and growth in structural members. This is done by enriching a standard finite element with extra degrees of freedom (DoF). However, most of these models either consider the translational load (achieved by very fine mesh with high computing cost), or are confined to thin shells with assumed full-depth cracks in a strong discontinuity sense [6-9].

For a reinforced slab the load causes coupled stretching and bending. Cracks are usually initiated at discrete positions and then propagated, until at last some localised full-depth cracks are formed. In this paper a non-linear layered FE procedure is developed for modelling of localised failure of reinforced concrete slabs under fire conditions. The layered procedure developed previously by Huang *et al.* [3] is enhanced with embedded *weak discontinuity* in which the strain is assumed to be discontinuous in cracked layers, but the displacement of the element is still assumed to be continuous.

2. FE PROCEDURE WITH EMBEDDED WEAK DISCONTINUITIES

2.1 Assumptions

The assumptions of the current procedure are extended from Mindlin-Reissner plate theory:

- The slab is assumed to be composed of perfectly bonded plain concrete or steel layers. The steel layers represent the equivalent reinforcing bars in the slab.
- A biaxial failure envelope is used to identify the initiation of cracking of concrete. Once a crack is initiated in a certain layer the directions of principal stresses and strains in that layer are fixed by the crack orientation. Further cracks in the element are either normal or parallel to the first crack. It is also assumed that the crack propagates from the initiating points to adjacent layers with the same crack orientation.

- A uniform cohesive cracking interface is assumed, which is governed by linear or bilinear traction-displacement softening curves. The magnitudes of the in-plane cracks are enriched with extra DoF.
- In order to represent the influence caused by the stress variation in high-order elements, each of the openings is decomposed onto integration points as virtually independent sub-cracks with the same orientation and length, determined by the initiation of cracking. The magnitude of each sub-crack is governed by the corresponding stress and strain status at this integration point. The total opening width of each layer in the element is then determined by summation across all integrating points.
- The total strain ε in the direction normal to the crack is decomposed into continuous $\tilde{\varepsilon}$ and discontinuous strains $\hat{\varepsilon}$. The continuous strain is associated with the deformation of the continuous (uncracked) element. The discontinuous strain describes the relative motion between two faces of the cracking interface. Standard FEM is applied for the continuous strain, and the discontinuous strain is transformed from the crack opening width *e* by means of scalable effective length of the element l_{eff}, which is the projection of the element on the normal to the crack direction [10, 11] as follows:

  $$\varepsilon = \tilde{\varepsilon} + \hat{\varepsilon} \tag{1}$$

  $$\hat{\varepsilon} = \gamma e / l_{eff} \tag{2}$$

  In which γ is the scale factor of the effective length, which is equal to the total number of integration points within the element.
- The coupling between the continuous solid and the discontinuous interface is enforced by means of the traction continuity condition across the crack interface. This provides an extra equation to condense the extra DoF (*e*) out from the stiffness matrix at element level. This condition can be expressed as

  $$\sigma = t \;\Rightarrow\; E\tilde{\varepsilon} = f_t + D_{nn}\, e \tag{3}$$

  where $t = f_t + D_{nn} e$ is a general expression for the surface traction along the cohesive crack, assuming a linear or bi-linear stress-displacement softening curve (further explanation is given in Section 2.3), f_t is the tensile strength of concrete, D_{nn} is the slope of the softening curve, and *E* is Young's modulus. From Eqns.(1-3), the opening width, *e*, is obtained as

  $$e = (E\varepsilon - f_t)/(D_{nn} + \gamma E / l_{eff}) \tag{4}$$

2.2 Development of the current FE model

2.2.1 Assumed Enhanced Strain (AES)

According to Eqn. (2), the equivalent discontinuous strain can be expressed in compact matrix form as

$$\hat{\boldsymbol{\varepsilon}}_n = \mathbf{M}_e \mathbf{e} \tag{5}$$

where,

$$\mathbf{M}_e = \begin{bmatrix} \alpha_n & 0 & 0 & 0 & 0 \\ 0 & \alpha_s & 0 & 0 & 0 \end{bmatrix}^T \tag{6}$$

$$\hat{\boldsymbol{\varepsilon}}_n = \{\hat{\varepsilon}_n \; \hat{\varepsilon}_s \; 0 \; 0 \; 0\}^T \tag{7}$$

$$\mathbf{e} = \{ e_n \; e_s \}^T \tag{8}$$

If the opening in direction *n* does not exist or is closed, then $\alpha_n = 0$. The same logic applies to the crack (if any) in direction *s*. Hence the matrix form of the continuous portion of the strain in the local (*n*-*s*) coordinate system can be expressed as

$$\tilde{\boldsymbol{\varepsilon}}_n = \mathbf{T}_\varepsilon \boldsymbol{\varepsilon} - \mathbf{M}_e \mathbf{e} \tag{9}$$

where $\boldsymbol{\varepsilon}$ is the total Green-Lagrange strain at any point in the element, expressed [3] as:

$$\boldsymbol{\varepsilon} = \begin{bmatrix} \mathbf{B}_m & z\mathbf{B}_b + \frac{1}{2}\mathbf{B}_L^b \\ 0 & \mathbf{B}_s \end{bmatrix} \mathbf{d} = \mathbf{B}^\varepsilon \mathbf{d} \tag{10}$$

in which *z* is the global coordinate; $\mathbf{B}_m$, $\mathbf{B}_b$ and $\mathbf{B}_s$ are generalized strain-displacement matrices related to linear small displacements; $\mathbf{B}_L^b$ is the strain-displacement matrix related to large displacements, and $\mathbf{d}$ is the total displacement vector. The details of $\mathbf{B}_m$, $\mathbf{B}_b$, $\mathbf{B}_s$ and $\mathbf{B}_L^b$ can be found in [3]; $\mathbf{T}_\varepsilon$ is the strain transformation matrix from global (*x*-*y*) to local (*n*-*s*) coordinates. Hence, the continuous strain in global (*x*-*y*) coordinate system can be represented as

$$\tilde{\boldsymbol{\varepsilon}}_x = \mathbf{T}_\varepsilon^{-1}\left(\mathbf{T}_\varepsilon \boldsymbol{\varepsilon} - \mathbf{M}_e \mathbf{e}\right) = \boldsymbol{\varepsilon} - \mathbf{T}_\varepsilon^{-1}\mathbf{M}_e \mathbf{e} \tag{11}$$

2.2.2 Force equilibrium across the crack interface

In Section 2.2.1, the extra degrees of freedom, **e**, were introduced as internal unknown parameters. Extra equations are needed to solve for these unknowns. The most natural requirement is that the traction vector across the crack should be equal to the stress tensor contracted with the crack normal at each integration point [11] as shown below,

$$\mathbf{M}_\sigma \boldsymbol{\sigma}_n = \{f_t\} + \hat{\mathbf{D}}\mathbf{e}_n \tag{12}$$

where, $\boldsymbol{\sigma}_n = \{\sigma_n \; \sigma_s \; \tau_{ns} \; \tau_{nt} \; \tau_{st}\}^T$ is the stress vector in the *n* and *s* directions; $\hat{\mathbf{D}}$ is the reference stiffness of the cohesive crack interface (see Section 2.3.1), and

$$\mathbf{M}_\sigma = \begin{bmatrix} \beta_n & 0 & 0 & 0 & 0 \\ 0 & \beta_s & 0 & 0 & 0 \end{bmatrix} \tag{13}$$

where β_n and β_s are 1 for an opened crack and 0 for an undamaged or closed interface in the local *n* and *s* directions, respectively; $\{f_t\} = \left\{f_t^n, \; f_t^s\right\}^T$ is the tensile strength vector of concrete.

Assuming that $\mathbf{D}'$ is the constitutive matrix of the continuous solid in local (*n-s*) coordinates, then Eqn. (12) becomes

$$\mathbf{M}_\sigma \mathbf{D}' \boldsymbol{\varepsilon}_n = \{f_t\} + \hat{\mathbf{D}}\mathbf{e} \tag{14}$$

Substituting Eqn. (9) into Eqn. (14), this equation becomes

$$\mathbf{M}_\sigma \mathbf{D}' \left(\mathbf{T}_\varepsilon \mathbf{B}^\varepsilon \mathbf{d} - \mathbf{M}_e \mathbf{e}\right) = \{f_t\} + \hat{\mathbf{D}}\mathbf{e} \tag{15}$$

To ensure that the derivative of $\hat{\mathbf{D}}$ is zero, a linear or bi-linear strain softening curve (see Section 2.3.1) is taken. A simple rearrangement of the linearization of Eqn. (15) leads to the relationship between the increments of crack openings $\dot{\mathbf{e}}$ and the nodal displacements $\dot{\mathbf{d}}$. That is

$$\dot{\mathbf{e}} = \left(\hat{\mathbf{D}} + \mathbf{M}_\sigma \mathbf{D}' \mathbf{M}_e\right)^{-1} \mathbf{M}_\sigma \mathbf{D}' \mathbf{T}_\varepsilon \mathbf{B} \dot{\mathbf{d}} \tag{16}$$

where

$$\mathbf{B} = \begin{bmatrix} \mathbf{B}_m & z\mathbf{B}_b + \mathbf{B}_L^b \\ 0 & \mathbf{B}_s \end{bmatrix} \tag{17}$$

2.2.3 Element stiffness matrix consistent with AES and traction continuity

Due to the fact that the crack interface is narrow compared with the element dimension (the stress tends to zero with the increment of opening width) it is assumed that the external forces are all resisted [11] by the continuous portion of the element. Thus, the internal nodal forces in the cracked element are evaluated from the standard relationship

$$\mathbf{f}_{\text{int}} = \int_V \mathbf{B}^T \boldsymbol{\sigma} dV \tag{18}$$

Linearization of Eqn. (18) leads to

$$\dot{\mathbf{f}}_{\text{int}} = \int_V \mathbf{B}^T \dot{\boldsymbol{\sigma}} dV + \int_V \dot{\mathbf{B}}^T \boldsymbol{\sigma} dV \tag{19}$$

The second term [3] on the right side of Eqn. (19) is

$$\int_V \dot{\mathbf{B}}^T \boldsymbol{\sigma} dV = \mathbf{K}_\sigma \dot{\mathbf{d}} \tag{20}$$

where $\mathbf{K}_\sigma$ is the geometric matrix.

From Eqns. (10), (11) and (16), the first term on the right side of Eqn. (19) can be expressed as

$$\int_V \mathbf{B}^T \dot{\boldsymbol{\sigma}} dV = \left(\int_V \mathbf{B}^T \mathbf{D}^w \mathbf{B} dV\right) \dot{\mathbf{d}} = \mathbf{K}^w \dot{\mathbf{d}} \tag{21}$$

with

$$\mathbf{D}^w = \mathbf{D}\left[\mathbf{I} - \mathbf{T}_\varepsilon^{-1} \mathbf{M}_e \left(\hat{\mathbf{D}} + \mathbf{M}_\sigma \mathbf{D}' \mathbf{M}_e\right)^{-1} \mathbf{M}_\sigma \mathbf{D}' \mathbf{T}_\varepsilon\right] \tag{22}$$

where **D** is the continuous constitutive matrix in the global coordinate system. It is assumed [3] that the integral concrete is isotropic, homogeneous and linearly elastic. A correction factor

k=6/5 is used to accoiunt for the effects of the parabolic shear stress distribution in the z direction. From Eqns. (19), (20) and (21) the element tangent stiffness matrix with embedded weak discontinuities is obtained as

$$\mathbf{K}_T = \mathbf{K}^w + \mathbf{K}_\sigma \tag{23}$$

2.3 Constitutive relationship

2.3.1 The cohesive law

In this research a Mode I crack model is adopted for simplicity. The initiation of cracks is based on a bi-axial concrete failure envelope [3]. After cracking, linear elastic behaviour is assumed in the continuous solid, but linear or bi-linear softening curves (Fig. 1) is assumed at the crack interface.

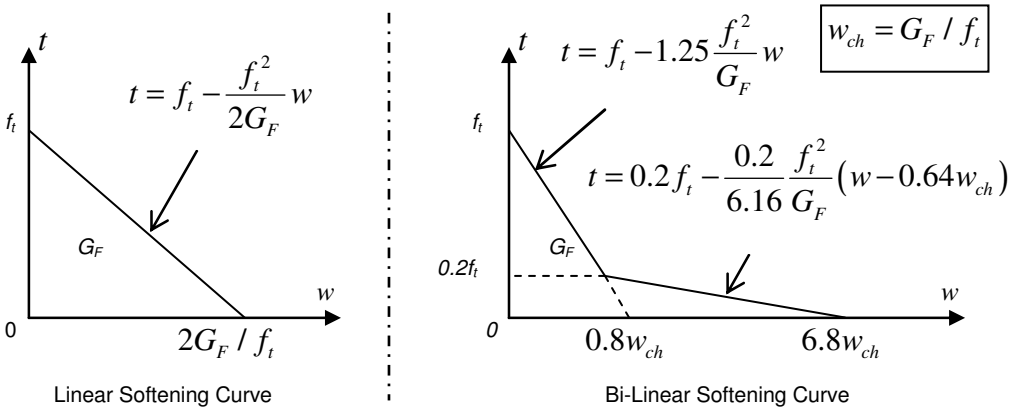

Fig. 1. Linear and Bi-linear tensile softening curves of concrete

Because of the orthotropic assumption after cracking, the principal stress and strain directions are assumed as fixed by the crack orientation. The reference stiffness matrix $\hat{\mathbf{D}}$ is 2x2:

$$\hat{\mathbf{D}} = \begin{bmatrix} D_{nn} & 0 \\ 0 & D_{ss} \end{bmatrix} \tag{24}$$

where, D_{nn} and D_{ss} are the tangent stiffnesses of the orthogonal cohesive crack interfaces in the n and s directions, respectively. Let $f(e,\kappa) = e - \kappa$ be the loading or unloading function, in which κ is the maximum normal opening width attained. Then $f \geq 0$ indicates loading (growing damage) and $f < 0$ indicates unloading (crack closing). For loading, D_{nn} and D_{ss} are derivatives of the softening function. For unloading, D_{nn} and D_{ss} are replaced by secant stiffnesses [12]. The governing equation of the increment of traction ($\dot{t}_n, \dot{t}_s$) across the cohesive crack interface is

$$\begin{Bmatrix} \dot{t}_n \\ \dot{t}_s \end{Bmatrix} = \begin{bmatrix} D_{nn} & 0 \\ 0 & D_{ss} \end{bmatrix} \begin{Bmatrix} \dot{e}_n \\ \dot{e}_s \end{Bmatrix} \tag{25}$$

where, $\dot{e}_n$, $\dot{e}_s$ are the increments of opening of the cohesive crack.

If the opening exceeds the traction-free opening width (according to the softening curve) the tangent reference stiffness is set to zero. If cracks are closed in both of the directions, then the undamaged material stiffness is regained.

2.3.2 The fracture energy

In the cohesive interface, the softening curve is governed by the fracture energy, which is a material property. In the *CEB-FIP Model Code* of 1990 [13], the fracture energy G_F (N/m) which is based on work-of-fracture, is a function of the compressive strength f_c of concrete (positive Mpa) and the maximum aggregate size d_a (mm). Bazant *et al.* [14] proposed a new fracture energy formulation in which the water-cement ratio w/c is also taken into account. The fracture energy is expressed as

$$G_F = 2.5\times\alpha_0\left(\frac{f_c}{0.051}\right)^{0.46}\left(1+\frac{d_a}{11.27}\right)^{0.22}\left(\frac{w}{c}\right)^{-0.30} \tag{26}$$

where $\alpha_0 = 1.0$ for rounded aggregates, and $\alpha_0 = 1.44$ for crushed or angular aggregates.

Fracture in reinforced concrete is somewhat different from that in plain concrete. In cracked reinforced concrete structures, reinforcement imparts some stress to the concrete between cracks via bonding action, so that this effectively leads to above-zero tensile stress existing in cracked concrete [15]. The mechanism commonly known as "tension stiffening" is usually assumed to be limited to a volume of concrete within 7.5 bar diameters from the reinforcement centre [13]. In this research, this phenomenon is considered by arbitrarily raising the fracture energy by 10% for concrete within the tension stiffening zone.

2.4 Extension of the current model to elevated temperatures

It is reasonable to keep the fracture energy constant when using numerical procedures at ambient temperature. However, the fracture energy of concrete changes at elevated temperatures and this should be considered in the model for fire conditions. In order to extend the model described above to elevated temperatures, the fracture energy is associated with temperature according to the *CEB-FIP Model Code* [13] as

$$G_F(T) = G_F^{T=20^0C}(1.06-0.003T) \tag{27}$$

where T is the temperature in °C.

In addition, the thermal strain ε_T of the material needs to be considered:

$$\varepsilon = \tilde{\varepsilon} + \hat{\varepsilon} + \varepsilon_T \tag{28}$$

Because the thermal strain is constant in each step of numerical analysis, then the crack opening width given by Eqn. (4), becomes at elevated temperatures

$$e = \frac{E(\varepsilon - \varepsilon_T) - f_t}{D_{nn} + \gamma E / l_{eff}} \tag{29}$$

2.5 Nonlinear iteration procedure

The Newton-Raphson iteration procedure is employed for non-linear analysis. Both geometric and material non-linearities are considered. The total loading or temperature rise for which the response of the structure is to be traced is divided into a number of steps. It is assumed that changes in the loads or temperatures occur only at the beginning or end of a step. During the iteration process, in any step the external loads and the temperatures in the layers of all elements are assumed to remain constant.

3. NUMERICAL STUDIES

Validation of the currently developed model is based on two series of small-scale reinforced concrete slab tests, carried out at the Universities of Manchester [1] and Sheffield [2]. The four experiments used here, at both ambient and elevated temperatures, are summarized in Table 1. All the slabs were simply supported and uniformly loaded, with all four corners clamped against lifting from the supports. No horizontal restraints were applied.

Test specimen	*Ambient Temperature*		*Elevated Temperatures*	
	M1 [1]	M2 [1]	MF1 [1]	FT10 [2]
Size (mm)	1800 x 1200	1200 x 1200	1800 x 1200	920 x 620
Size in support (mm)	1700 x 1100	1100 x 1100	1700 x 1100	850 x 550
Thickness (mm)	18.2	19.1	19.7	24
Diameter of steel bar (mm)	2.42	2.42	2.43	0.71
Spacing of steel bar (mm)	50.8	50.8	50.8	
Yield strength of steel f_y (MPa)	732	732	722	250
Concrete strength f_{cu} (MPa)	41.3	38	43.2	39
Concrete cover (mm)	5	5	5	7.5
Water-cement ratio	0.3	0.3	0.3	0.47
Maximum aggregate size (mm)	6	6	6	4
Yield line load (kN/m^2)	8.52	13.80	9.52	2.49

Table 1. Experimental data used for validation

The material properties provided above were used for numerical analysis. Comparisons of the central deflections of numerical and test results of these slabs are shown in Figs. 2 to 5. It can be seen from these results that the current model can be used to predict the global behaviour, as

well as the progressive integrity failure of reinforced concrete slabs at both ambient and elevated temperatures. Also, the numerical results are neither mesh- nor aspect-ratio-sensitive.

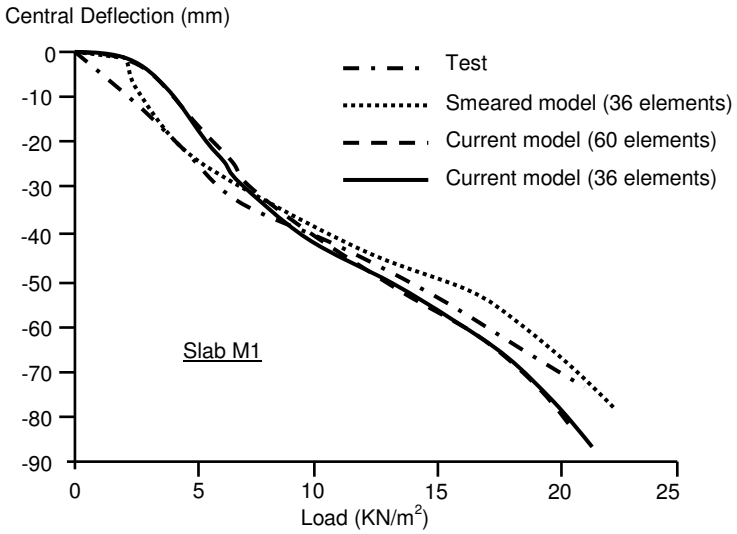

Fig. 2. Comparison of predicted and measured central deflections of slab M1 [1] using different meshes.

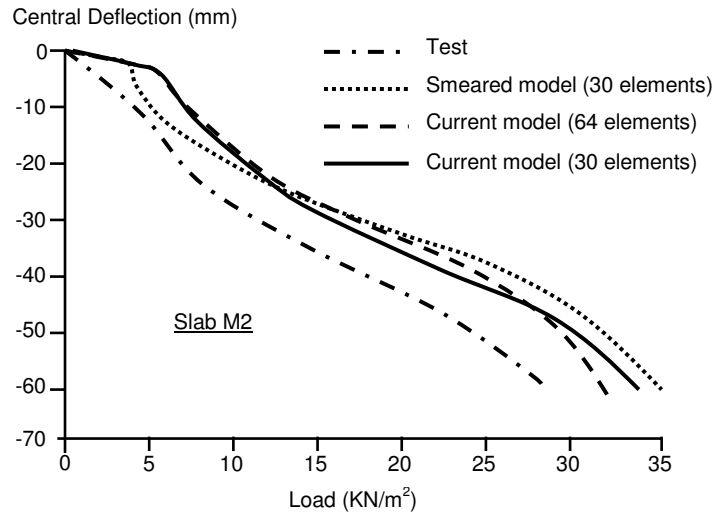

Fig. 3. Comparison of predicted and measured central deflections of slab M2 [1] using different meshes.

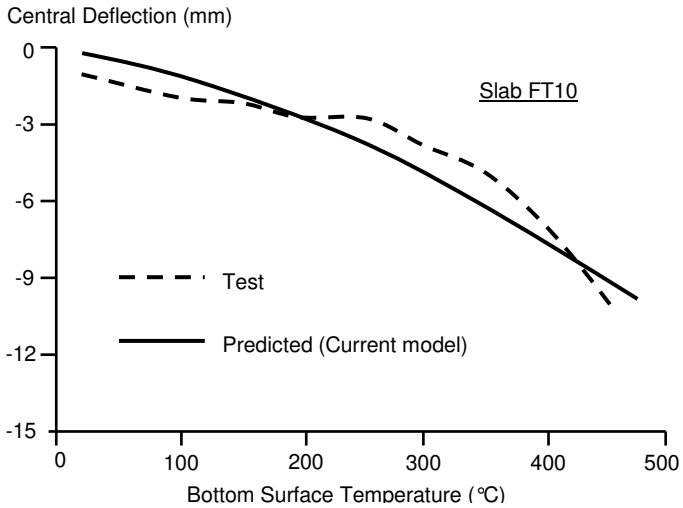

Fig. 4 Comparison of predicted and measured central deflections of slab FT10 [2]

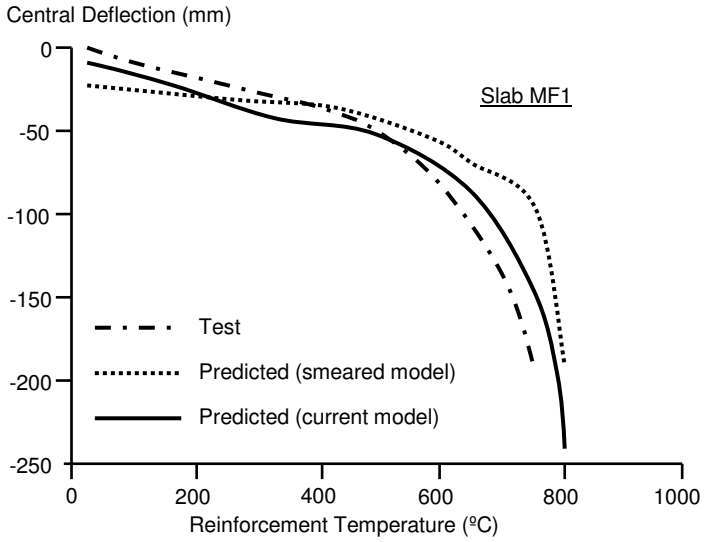

Fig. 5 Comparison of predicted and measured central deflections of slab MF1 [1].

4. CONCLUSIONS

A new layered slab element model has been developed to model the localised failure of reinforced concrete slabs subject to large deflections. The previous non-linear layered procedure developed at the University of Sheffield [3] has been enhanced with embedded weak discontinuities. The total strain is decomposed into continuous and discontinuous strains. The continuous strain is associated with the deformation of the elements as if the element is

uncracked, and the discontinuous strain is converted from the opening width of the crack by means of an element effective length. The magnitude of a crack is modelled by extra DoF, which is enforced by traction continuity across the uniform cohesive crack interface. In order to account for the stress variation in an element, the discontinuity is decomposed into virtual sub-cracks which are governed by the corresponding stress and strain states at the integration points. The validations show that the model can predict the global behaviour of slabs, as well as the progressive growth of individual cracks, at both ambient and elevated temperatures with reasonable accuracy. A comparison of the predicted and actual cracking of the slab MF1 is shown in Figs. 6 and 7.

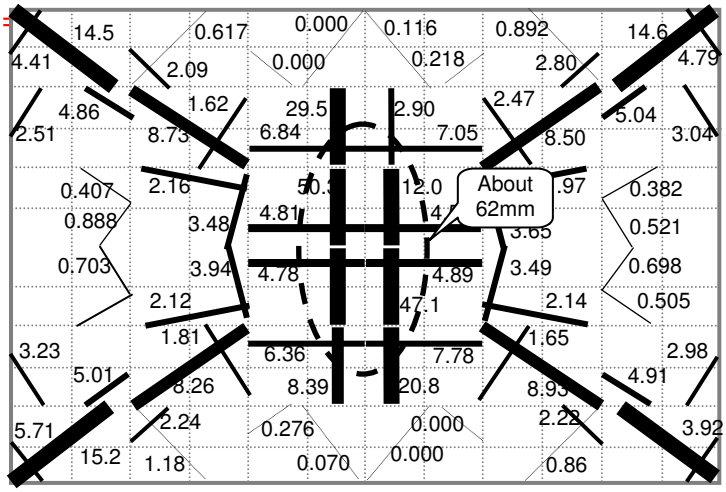

Fig. 6. Predicted cracking pattern of the bottom layer of slab MF1 at 800°C of reinforcement temperature (all units in mm).

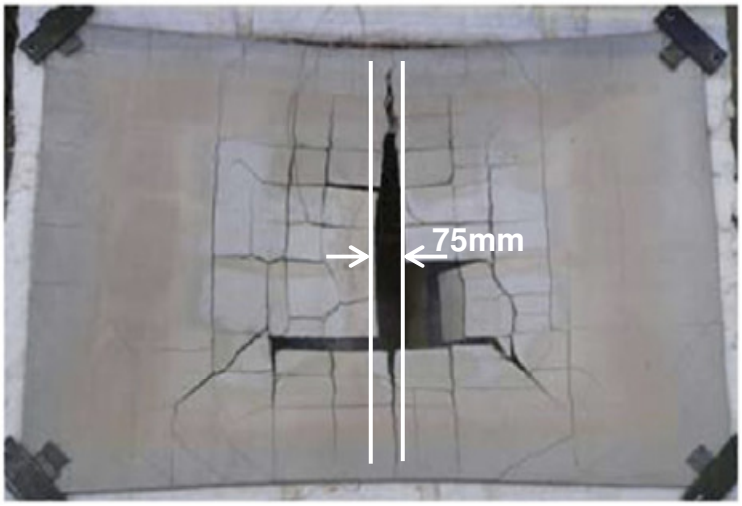

Fig. 7. Tested cracking pattern of the top surface of slab MF1 [1].

The predicted cracking pattern agrees well with the experiment results. The validation also shows that this approach is not sensitive to element mesh size or the aspect ratio of the slab. This model can be used for performance-based structural fire engineering design of reinforced concrete slabs, although further research is needed to determine how the bond characteristic between concrete and reinforcing steel can be included in futurel.

5. REFERENCES

[1] Bailey, C.G. and Toh, W.S., "Small-scale concrete slab tests at ambient and elevated temperatures", *Engineering Structures,* (2007), in press (doi: 10.1016 / j.engstruct.2007.01.023).

[2] Foster, S., "Tensile membrane action of reinforced concrete slabs at ambient and elevated temperatures", *PhD thesis*, Department of Civil and Structural Engineering, University of Sheffield, 2006.

[3] Huang, Z., Burgess, I.W. and Plank, R.J., "Modelling Membrane Action of Concrete Slabs in Composite Buildings in Fire. Part I: Theoretical Development", *Journal of Structural Engineering*, **129** (8), (2003), pp1093-1102.

[4] Gillie, M. et al., "Modelling of heated composite floor slabs with reference to Cardington experiments", *Fire Safety Journal,* **36**, (2001) pp745-767.

[5] Lim, L. et al., "Numerical modelling of two-way reinforced concrete slabs in fire", *Engineering Structures*, **26**,(2004) pp1081-1091.

[6] Jirasek M., Belytschko T., "Computational resolution of strong discontinuities", *5th World Congress on Computational Mechanics*, Vienna, Austria. 2002. Eds.: H.A. Mang, F.G. Rammerstorfer, J. Eberhardsteiner.

[7] Fan S.C., Liu, X., and Lee, C.K., "Enriched partition-of-unity finite element method for stress intensity factors at crack tips", *Computers and Structures,* **82**, (2004), pp. 445-461.

[8] Sukumar, N. and Prevost, J.H., "Modeling quasi-static crack growth with the extended finite element method Part I: Computer implementation", *International Journal of Solids and Structures*, **40**, (2003), pp.7513–7537.

[9] Areias, P.M.A. and Belytschko, T., "Non-linear analysis of shells with arbitrary evolving cracks using XFEM", *Int. J. Numerical Methods in Engineering*, **62**, (2005), pp.384-415.

[10] Bazant, Z.P. and Oh, B.H., "Crack band theory for fracture of concrete", *Material and Structures*, **16**, (1983), pp155-177.

[11] Jirasek, M. and Zimmermann, T., "Embedded crack model: I. Basic formulation", *Int. J. Numerical Methods in Engineering*, **50**, (2001), pp1269-1290.

[12] Wells, G.N. and Sluys, J., "Three-dimensional embedded discontinuity model for brittle fracture", *International Journal of Solids and Structures*, **38**, (2001), pp.897-913.

[13] CEB-FIP Model Code: *Comite Euro-International du Beton*, Bulletin D'information No. **213/214**, Tomas Telford, London, May 1993.

[14] Bazant, Z.P. and Becq-Giraudon, E., "Statistical prediction of fracture parameters of concrete and implications for choice of testing standard", *Cement and Concrete Research,* **32**, (2002), pp529-556.

[15] Yamamoto, T. and Vecchio, F., "Analysis of reinforced concrete shells for transverse shear and torsion", *ACI Structural Journal*, **98**, (2001), pp 191-200.